IEEE Access
Multidisciplinary | Rapid Review | Open Access Journal

Received 29 August 2023, accepted 14 September 2023, date of publication 19 September 2023,
date of current version 25 September 2023.

Digital Object Identifier 10.1109/ACCESS.2023.3317180

RESEARCH ARTICLE

Design of Permutation Index DCSK With Noise Reduction for Short-Range IoT Communications

BINGRUI WANG[1], HAOYU CHEN[2], (Student Member, IEEE), ZHAOPENG XIE[2], XIAOPU MA[1], AND ZIQIANG ZHU[2]

[1]Henan Intelligent Engineering Research Center, Nanyang Normal University, Nanyang, Henan 473061, China
[2]School of Advanced Manufacturing, Fuzhou University, Jinjiang, Fujian 362251, China

Corresponding author: Zhaopeng Xie (xzp_fzu@163.com)

This work was supported in part by the NSF of China under Grant 62171135, in part by the Fujian Distinguished Talent Project under Grant 2022J06010, in part by the Project of Science and Technology of Quanzhou City under Grant 2021N050, and in part by the Key Industrial Software Project in Fujian Province 2022.

ABSTRACT In this paper, we propose a permutation index differential chaos shift keying with the noise reduction (NR-PI-DCSK) to alleviate the negative effect of the additive noise and fading interference. Instead of sending a β-length chaotic sequence as the reference in the conventional PI-DCSK, the transmitter of NR-PI-DCSK generates β/R chaotic samples and repeats R times, which serve as the reference sequence. The permuted copy of the reference is used to carry the data given the predefined permutation index. After the correlation and averaging of these R chaotic segments at the receiver, the variance of noise and fading can be greatly reduced and the performance is improved. Then, we derive the analytical BER expressions for the multipath fading channels, which are verified by the consistent simulations. The results show that the proposed NR-PI-DCSK can achieve up to 3 dB performance gain over the conventional PI-DCSK in different wireless fading channels. In addition, the performance advantage of the proposed NR-PI-DCSK is also demonstrated in a typical UWB channel by simulations. More importantly, the proposed scheme maintains almost the same low transceiver complexity as the conventional ones, since it only requires the correlators. Thus, the NR-PI-DCSK can be seen as a promising candidate for low-cost short-range IoT communications.

INDEX TERMS Differential chaos shift keying (DCSK), permutation index (PI), noise reduction (NR), performance analysis.

I. INTRODUCTION

With its outstanding characteristics, the chaotic signal is naturally suited for spread-spectrum (SS) communication systems [1]. In particular, chaos-based communications provide excellent robustness against multipath fading [2] and jamming [3]. This has motivated enormous researches on chaotic communication, where the differential chaos shift keying (DCSK) was particularly widely studied due its low-complexity and performance advantages. Although this non-coherent DCSK modulation performs worse than coherent BPSK/QPSK modulations in AWGN channels [4], it is suitable for special wireless applications such as WLAN and industrial IoT applications that require no complex synchronization, low transmitted power spectral density to avoid telecommunication interfering, and robustness against multipath propagation and industrial disturbances [4], [5], [6]. Note that the chaotic signal can be generated by digital chaotic map [1] or memristor chaotic system [5], [6]. The performance of DCSK was further analyzed in [41] over different channel models. DCSK has been developed and updated to cater for various scenarios, such as ultra-wideband (UWB) communication [8], continuous-mobility system [9], powerline communication (PLC) system [10], and e-Health IoT systems [11]. To ensure reliable transmission, channel coding has been applied into the DCSK-based communications [12], [13], [14]. However, the conventional DCSK suffers from both low data rate and low energy

The associate editor coordinating the review of this manuscript and approving it for publication was Amjad Mehmood.

efficiency, since two consecutive time slots are required to send a data bit in a symbol duration [15], [16]. Besides, the receiver of DCSK needs the radio frequency delay line to recover the information bits.

To remove the delay line, the time reversal operation was adopted to the chaotic sequence in I-DCSK [17]. The receiver of I-DCSK only needs to correlate the received signal with its time reversal version to estimate the transmitted bits. By leveraging the multi-carrier communication, the multi-carrier DCSK (MC-DCSK) used a subcarrier to send the reference, while the remaining subcarriers to send the information sequence [18]. By utilizing the orthogonality of the Walsh code, the code shifted DCSK (CS-DCSK) and its generalised version (GCS-DCSK) have been proposed in [19] and [20]. To improve the energy efficiency, the differentially DCSK (DDCSK) and the short reference DCSK (SR-DCSK) have been investigated in [21], [22], respectively. Moreover, [23], a deep learning (DL)-based demodulation was proposed for DCSK systems, which is efficient for applications with problematic channel estimation. For secure communications, a reconfigurable intelligent surface (RIS)-aided M-ary DCSK with block interleaving (RIS-MDCSK-BI) system is proposed, where a pair of block interleaving patterns are used to enhance security performance [24].

Moreover, Index modulation (IM) is regraded as the appealing solution to high-data-rate wireless communications, which achieves performance gains with less cost [25]. Extra information bits in IM-based communications can be sent through predefined patterns, e.g., frequency and antenna [26]. Thus, this technique provides insights into boosting the data rate of DCSK-based communications. Different from MC-DCSK, parts of predefined subcarriers are deployed for information sequence in carrier index DCSK (CI-DCSK) [27]. Furthermore, its high-data-rate version, namely HDR-CI-DCSK, was proposed to enhance the spectral efficiency (SE), data rate as well as bit error rate (BER) performance [28]. By applying the code index modulation [29], CIM-DCSK was proposed to carry additional bits through Walsh code [30] and its enhanced version was designed in [31]. By exploiting the properties of chaotic signal, the permutation index DCSK (PI-DCSK) has been used to send extra information bits [32]. In particular, a β-length chaotic signal is sent in the first time slot as the reference and the information sequence, i.e., the permuted replica of the reference sequence, is sent in the following time slot. In [33], a reference-modulated PI-DCSK (RM-PI-DCSK) was proposed to carry one more modulation bit in the reference segment than the conventional PI-DCSK. To achieve high-data-rate transmissions, a new index-modulation-aided DCSK (CTIM-DCSK) system was developed, where the orthogonal sinusoidal carriers are used to send both the reference and the information signals [34].

Although PI-DCSK can effectively enhance the data rate by transmitting extra bits on permutation index, the addition of channel noise to both the reference signal and the permutated data-bearing signal deteriorates its error performance. Thus, in this paper, we exploit the noise reduction (NR) technique [35] in PI-DCSK to form NR-PI-DCSK, which can reduce the average noise variance in the demodulation and then improve performance. Similar to conventional PI-DCSK, the reference sequence is permuted to form the data-bearing sequence, where the permutation index is selected by the transmitted bits. In this way, we can transmit and estimate the extra information by determining the permutation index at the receiver. The resultant signal is correlated with its permuted replicas to estimate the transmitted bits. Due to the frame format of the NR-PI-DCSK and the average filter at the receiver, the variance of the noise can be sharpened and lead to performance improvement. Also, the analytical BER expressions of NR-PI-DCSK over multipath Rayleigh fading channel are derived and confirmed with the simulation results. Finally, we compare the proposed system with PI-DCSK over two different channel models to show its performance advantages.

The rest of paper is organized as follows. Section II introduces model of the NR-PI-DCSK system. Section III compares and analyzes the simulation results. Section IV draws the conclusions.

II. SYSTEM MODEL

A. ARCHITECTURE OF TRANSCEIVER

As shown in Fig. 1, the chaotic generator sends a β/R-length chaotic vector $\mathbf{x} = [x_1, x_2, \ldots, x_{\beta/R}]$ to the buffer. This length-β/R signal $\mathbf{x}$ can be generated by the logistic mapping, i.e.,

$$x_{k+1} = 1 - 2x_k^2, \tag{1}$$

To obtain a length-β chaotic signal $\mathbf{S}$, we replicate this $\mathbf{x}$ with β/R samples by R times. This process is given by

$$\mathbf{S} = \mathbf{1}_{1\times R} \otimes \mathbf{x}, \tag{2}$$

where $\otimes$ denotes the Kronecker product and $\mathbf{1}_{1\times R} = [1, 1, \ldots, 1]$. The frame format of the chaotic samples is illustrated in Fig. 2.

At the transmitter, the input bits in the j-th group is divided into two parts. The first part includes a modulated bit and the second part includes m_c mapped bits. Then, the modulated bit and mapped bits are converted to the modulated symbol b_j and the mapped symbol a_j, respectively. It should be noted that the mapped symbol a_j is used to choose corresponding permuted replicas $P_{a_j}(\mathbf{S})$ from the permutation block and the modulated symbol b_j is served to inverse or maintain the polarity of $P_{a_j}(\mathbf{S})$, i.e., $b_j P_{a_j}(\mathbf{S})$, $b_j \in \{-1, +1\}$. Those predefined permutations should be select properly to avoid the interference of different chaotic signals, i.e.,

$$P_i(\mathbf{S})\,\mathbf{S}^T \approx 0, \tag{3}$$

$$P_i(\mathbf{S})\,P_{i'}(\mathbf{S})^T \approx 0, \quad \text{for } i \neq i', \tag{4}$$

where $(\cdot)^T$ is the transposition operation. Actually, in practical implementation, most chaotic mappings degrade due

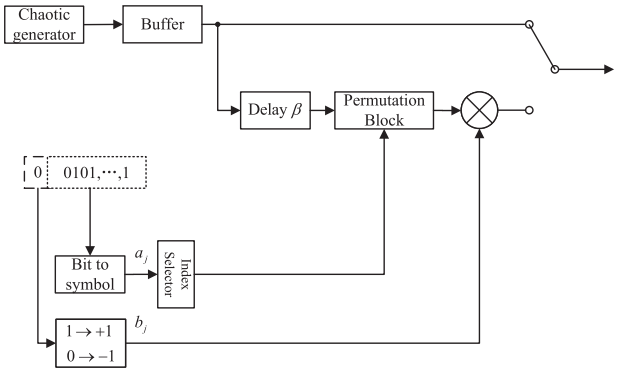

FIGURE 1. Block diagram of the NR-PI-DCSK transmitter.

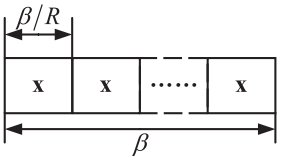

FIGURE 2. Frame formats of the chaotic samples in NR-PI-DCSK.

to the finite representation [36]. This issue can be partly addressed by using high precision hardware and complex control algorithm [37], while a more recent study [38] used digital FIR filters for the chaotic shaping filter to encode information into the chaotic waveform.

In a NR-PI-DCSK symbol duration, the reference sequence $\mathbf{S}$ is sent in the first time slot, the information sequence is sent in the second time slot. The transmitted sequence $\mathbf{e}$ is then given by

$$\mathbf{e} = \left[\mathbf{S}, b_j P_{a_j}(\mathbf{S})\right]. \tag{5}$$

In this paper, we consider a commonly used multipath Rayleigh fading channel model. The received signal $\mathbf{r}$ at the receiver is given by

$$\mathbf{r} = \sum_{l=1}^{L} \alpha_l \mathbf{e}_{\tau_l} + \mathbf{n}, \tag{6}$$

where $\mathbf{e}_{\tau_l}$ is a replica of transmitted sequence $\mathbf{e}$ delay by τ_l. $\mathbf{n} = \left[n_1, n_2, \ldots, n_{2\beta}\right]$ is the additive white Gaussian noise (AWGN) and n_k is the sample with zero mean and variance $N_0/2$. In (6), α_l denotes the channel coefficient in the l-th path that follows the Rayleigh distribution. The probability density function (PDF) of α_l is given by

$$f(\alpha|\xi) = \frac{\alpha}{\xi^2} e^{-\frac{\alpha^2}{2\xi^2}}, \tag{7}$$

where ξ is the positive distribution scale parameter.

The block diagram of NR-PI-DCSK receiver is shown in Fig. 3. The received signal passes through the average filter with a size of β/R. The received reference sequence after averaged is sent to the permutation block and then 2^{m_c} replicas are gotten. The averaged information sequence is simultaneously correlated with those 2^{m_c} replicas over the duration β/R, i.e., 2^{m_c} decision variables are obtained. The decision variable $I_{j,\hat{i}}$ of the j-th group at the $\hat{i}$-th correlator when $\hat{i} = a_j$, can be computed as

$$I_{j,\hat{i}} = \sum_{k=1}^{\beta/R} \left(\sum_{l=1}^{L} \alpha_l P_{\hat{i}}\left(x_{k-\tau_l}\right) + \underbrace{\frac{1}{R}\sum_{r=1}^{R} n_{k+(r-1)\frac{\beta}{R}}}_{N_{1,k}} \right) \times \left(\sum_{l=1}^{L} \alpha_l b_j P_{a_j}\left(x_{k-\tau_l}\right) + \underbrace{\frac{1}{R}\sum_{r=1}^{R} n_{k+\beta+(r-1)\frac{\beta}{R}}}_{N_{2,k}} \right). \tag{8}$$

Similarly, for $i \neq a_j$, the decision variable at the i-th correlator can be expressed as

$$I_{j,i} = \sum_{k=1}^{\beta/R} \left(\sum_{l=1}^{L} \alpha_l P_i\left(x_{k-\tau_l}\right) + \underbrace{\frac{1}{R}\sum_{r=1}^{R} n_{k+(r-1)\frac{\beta}{R}}}_{N_{1,k}} \right) \times \left(\sum_{l=1}^{L} \alpha_l b_j P_{a_j}\left(x_{k-\tau_l}\right) + \underbrace{\frac{1}{R}\sum_{r=1}^{R} n_{k+\beta+(r-1)\frac{\beta}{R}}}_{N_{2,k}} \right). \tag{9}$$

It should be noted that for the variance of the averaged noise term in (8) and (9) (i.e., $N_{1,k}$ and $N_{2,k}$) are computed as

$$\mathrm{var}\left\{N_{1,k}\right\} = \mathrm{var}\left\{N_{2,k}\right\} = \frac{\mathrm{var}\left\{n_k\right\}}{R} = \frac{N_0}{2R}. \tag{10}$$

where $\mathrm{var}\{\cdot\}$ represents the variance operator. The variance of the noise is sharpened at the receiver by the average operation, which equivalently increases the received SNR and then leads to performance improvement.

To estimate the mapped symbol $\hat{a}_j$, the outputs of 2^{m_c} correlators are compared to find the maximum absolute value, i.e.,

$$\hat{a}_j = \arg\max_i \left(\left|I_{j,i}\right|\right), i = 1, \cdots, 2^{m_c}. \tag{11}$$

The modulated symbol $\hat{b}_j$ can then be estimated by the sign of the selected correlator output $I_{j,\hat{a}_j}$ as

$$\hat{b}_j = \mathrm{sign}\left(I_{j,\hat{a}_j}\right). \tag{12}$$

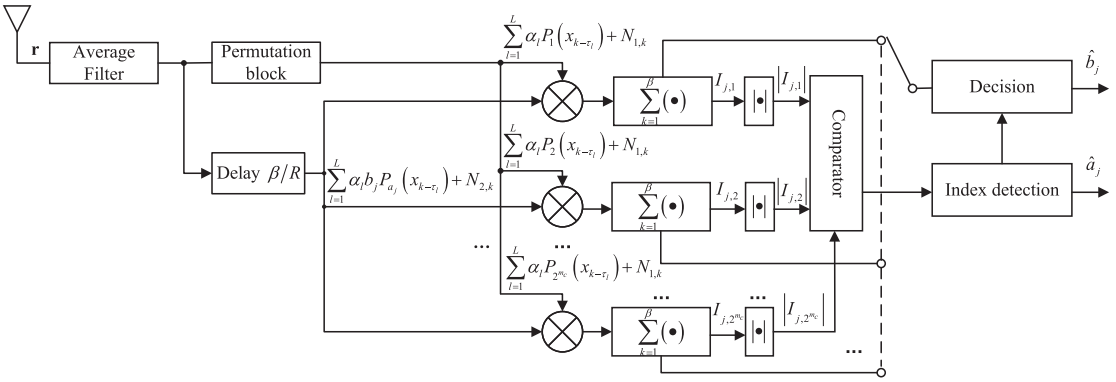

FIGURE 3. Block diagram of the NR-PI-DCSK receiver.

B. ENERGY EFFICIENCY ANALYSIS

To analyze the energy efficiency of NR-PI-DCSK, we introduce the data-energy-to-bit-energy ratio (DBR) as [32]

$$\mathrm{DBR} = \frac{E_d}{E_b}, \tag{13}$$

where E_d denotes the transmitted energy of the information sequence and E_b denotes the energy of sending a information bit. In the proposed design, the symbol energy E_s can be calculated as

$$E_s = E_d + E_r. \tag{14}$$

where E_r is the energy of sending the reference sequence. Moreover, recall that the information sequence in the second time slot is the permuted replica of the reference, we then have

$$E_r = E_d = R\sum_{k=1}^{\beta/R} x_k^2. \tag{15}$$

Thus, the symbol energy E_s of the NR-PI-DCSK is

$$E_s = 2R\sum_{k=1}^{\beta/R} x_k^2. \tag{16}$$

In addition, since $m_c + 1$ bits are sent in a NR-PI-DCSK symbol duration, the bit energy E_b is computed by

$$E_b = \frac{E_s}{m_c+1} = \frac{2R\sum_{k=1}^{\beta/R} x_k^2}{m_c+1}. \tag{17}$$

According to (13)-(17), the DBR of the proposed NR-PI-DCSK can be computed as

$$\mathrm{DBR} = \frac{m_c+1}{2}. \tag{18}$$

III. PERFORMANCE ANALYSIS

In this section, we derive the analytical BER performance of the NR-PI-DCSK over the multipath Rayleigh fading channel.

A. BER ANALYSIS OF NR-PI-DCSK

In a NR-PI-DCSK symbol duration, $m_c + 1$ bits are sent, including m_c mapped bits transmitted by permutation index and a modulated bit transmitted by DCSK. The total BER P_T of NR-PI-DCSK is comprised of the BER of modulated bits $P_{e\mathrm{mod}}$ and the BER of mapped bits $P_{e\mathrm{ind}}$, given by

$$P_T = \frac{m_c}{(m_c+1)}P_{e\mathrm{ind}} + \frac{1}{(m_c+1)}P_{e\mathrm{mod}}. \tag{19}$$

The BER of the mapped bits $P_{e\mathrm{ind}}$ can be computed by the number of mapped bits m_c and the probability of erroneous permutation detection P_{ed} according to [40]

$$P_{e\mathrm{ind}} = \frac{2^{(m_c-1)}}{2^{m_c}-1}P_{ed}. \tag{20}$$

Note that the recovery of the physically modulated symbol relies on both the permutation recovery and the despreading. We can see that there are two different cases that result in error detection. In the first case, the permutation index symbol is recovered correctly but an error exists in the estimation of the modulated symbol. The probability of this erroneous detection $P_{e\mathrm{DCSK}}$ is given by [1]

$$P_{e\mathrm{DCSK}} = \frac{1}{2}\mathrm{erfc}\left(\frac{E\left\{I_{j,\hat{i}}\right\}}{\sqrt{2\,\mathrm{var}\left\{I_{j,\hat{i}}\right\}}}\right), \tag{21}$$

where $E\{\cdot\}$ the expectation operator and $\mathrm{erfc}(\cdot)$ is the complementary error function.

In the second case, the estimation of the permutation index is wrong. Thus, the probability of correct modulated symbol detection equals 1/2. In this vein, the BER of the modulated symbol is computed as

$$P_{e\mathrm{mod}} = P_{e\mathrm{DCSK}}(1-P_{ed}) + 0.5P_{ed}. \tag{22}$$

B. DERIVATION OF P_{ED}

Assuming that the modulated symbol $b_j = +1$ and permutation index symbol $a_j = \hat{i}$ are sent at the transmitter. For large β/R, the time-shift term in (8) and (9) can be

neglected due to the near-orthogonality of the different chaotic signals, given by

$$\sum_{k=1}^{\beta/R} x_{k-\tau_l} x_{k-\tau_{l'}} \approx 0 \text{ for } l \neq l'. \tag{23}$$

Thus, the expectation and the variance of $I_{j,\hat{i}}$ and $I_{j,i}$ can be approximately computed as

$$\mu_1 = E\left\{I_{j,\hat{i}}\right\} \approx N_0 \frac{\gamma_b (m_c+1)}{2R}, \tag{24}$$

$$\sigma_1^2 = \text{var}\left\{I_{j,\hat{i}}\right\} \approx N_0^2 \left(\frac{\gamma_b (m_c+1)}{2R^2} + \frac{\beta}{4R^3}\right), \tag{25}$$

$$\mu_2 = E\left\{I_{j,i}\right\} \approx 0, \tag{26}$$

$$\sigma_2^2 = \text{var}\left\{I_{j,i}\right\} \approx N_0^2 \left(\frac{\gamma_b (m_c+1)}{2R^2} + \frac{\beta}{4R^3}\right). \tag{27}$$

where γ_b is the SNR per bit over L-path Rayleigh fading channels, given by

$$\gamma_b = \frac{E_b}{N_0} \sum_{l=1}^{L} \alpha_l^2. \tag{28}$$

According to (8) and (9), we can see that the absolute decision variables $\left|I_{j,\hat{i}}\right|$ and $\left|I_{j,i}\right|$ follow identical folded normal distribution. The PDF of variable $\left|I_{j,\hat{i}}\right|$ and cumulative distribution function (CDF) of variable $\left|I_{j,i}\right|$ are respectively

$$g_{\left|I_{j,\hat{i}}\right|}(w) = \frac{1}{\sqrt{2\pi\sigma_1^2}} \left[e^{-\frac{(w-\mu_1)^2}{2\sigma_1^2}} + e^{-\frac{(w+\mu_1)^2}{2\sigma_1^2}}\right], \tag{29}$$

and

$$G_{|I_{j,i}|}(w) = \text{erf}\left(\frac{w}{\sqrt{2\sigma_2^2}}\right). \tag{30}$$

Thus, the probability of erroneous permutation index symbol detection P_{ed} is

$$\begin{aligned} P_{ed} &= \Pr\left(\left|I_{j,\hat{i}}\right| < \max_{\substack{i\in\{1,\cdots,2^{m_c}\} \\ i\neq\hat{i}}} \left\{\left|I_{j,i}\right| \middle| P_i\right\}\right) \\ &= \int_0^\infty \left\{1 - \left[G_{|I_{j,i}|}(w)\right]^{2^{m_c}-1}\right\} g_{\left|I_{j,\hat{i}}\right|}(w)\, dw \\ &= \frac{1}{\sqrt{2\pi\sigma_1^2}} \int_0^\infty \left\{1 - \left[\text{erf}\left(\frac{w}{\sqrt{2\sigma_2^2}}\right)\right]^{2^{m_c}-1}\right\} \\ &\quad \times \left[e^{-\frac{(w-\mu_1)^2}{2\sigma_1^2}} + e^{-\frac{(w+\mu_1)^2}{2\sigma_1^2}}\right] dw \xrightarrow{z=\frac{w}{N_0}} \\ &= \frac{1}{\sqrt{2\pi C}} \int_0^\infty \left\{1 - \left[\text{erf}\left(\frac{z}{\sqrt{2D}}\right)\right]^{2^{m_c}-1}\right\} \\ &\quad \times \left[e^{-\frac{\left(z-\frac{(m_c+1)}{2R}\gamma_b\right)^2}{2C}} + e^{-\frac{\left(z+\frac{(m_c+1)}{2R}\gamma_b\right)^2}{2C}}\right] dz, \end{aligned} \tag{31}$$

where, $C = D = \frac{\gamma_b(m_c+1)}{2R^2} + \frac{\beta}{4R^3}$.

Finally, the averaged BER of the NR-PI-DCSK over multipath Rayleigh fading channels can be given by

$$\bar{P}_T = \int_0^\infty P_T g(\gamma_b) d\gamma_b. \tag{32}$$

where $g(\gamma_b)$ denotes the PDF of SNR γ_b. For the channel model that distribution of power gain is equal (i.e., $E\left\{\alpha_l^2\right\} = 1/L$), the PDF of γ_b is expressed as

$$g(\gamma_b) = \frac{\gamma_b^{L-1}}{\bar{\gamma}^L (L-1)!} e^{-\frac{\gamma_b}{\bar{\gamma}}}, \tag{33}$$

where $\bar{\gamma} = E\left\{\alpha_l^2\right\} E_b/N_0$ denotes the received SNR each path. For the channels with dissimilar power gains, the PDF of γ_b is given by

$$g(\gamma_b) = \sum_{l=1}^{L} \frac{\varphi_l}{\bar{\gamma}_l} e^{-\frac{\gamma_b}{\bar{\gamma}_l}}, \tag{34}$$

where

$$\varphi_l = \prod_{\substack{\mu=1 \\ \mu\neq l}}^{L} \frac{\bar{\gamma}_l}{\bar{\gamma}_l - \bar{\gamma}_\mu}. \tag{35}$$

IV. SIMULATION AND ANALYSIS

In this section, we evaluate the BER performance of the NR-PI-DCSK. Two different multipath Rayleigh fading channels are used in the simulation. In the first channel model, namely CM1 channel, two-path channel with power gain of $E\left\{\alpha_1^2\right\} = E\left\{\alpha_2^2\right\} = \frac{1}{2}$ and path delays $\tau_1 = 0$, $\tau_2 = 1$ is used. The second channel model, namely CM2 channel, uses three-path channel with unequal power gain $E\left\{\alpha_1^2\right\} = 4/7$, $E\left\{\alpha_2^2\right\} = 2/7$, $E\left\{\alpha_3^2\right\} = 1/7$ and path delays $\tau_1 = 0$, $\tau_2 = 1$, $\tau_3 = 2$.

Fig. 4 demonstrates the numerical and simulated results of the proposed NR-PI-DCSK for different R and $\beta = 200$ over CM1 and CM2 channels. We can see that the increasing R can lead to a lower BER level given a β. The reason for this lies in that the averaged operation reduces the variance of additive noise as R increases, as in (10). With respect to the results in CM1 channel, the performance gain of the proposed scheme over PI-DCSK (i.e., $R = 1$) reaches to 3.2 dB at a BER of 10^{-4}. In Fig. 5, we evaluate the impact of the number of mapped bits m_c on the error performance. It shows that the scheme with $m_c = 3$ outperform the ones with the less m_c, i.e., $m_c = 2$ and $m_c = 1$. This is because that more bits are sent in a symbol suggests enhanced bit energy against the noise given a total transmit energy. At a BER of 10^{-4}, we see that proposed scheme with $m_c = 3$ achieves a performance gain of 1.5 dB over that with $m_c = 1$ over CM2 channel. Also, as viewed in Figs. 4 and 5, the numerical results highly consist with the simulations for both channel models. As shown in Fig. 6, with $m_c = 3$ and $M = 16$, the proposed NR-PI-DCSK can achieve a performance gain of 2 dB over PT-CIM-DCSK [31] at a BER of 10^{-4}. The performance gain comes from the fact that the noise variance is effectively reduced using the average noise filter.

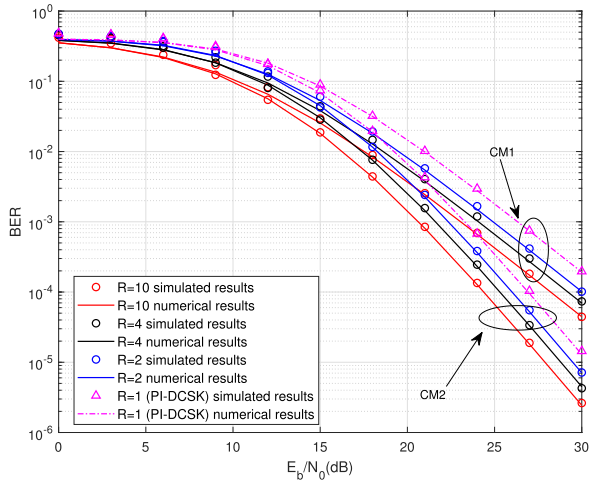

FIGURE 4. Error performance of the NR-PI-DCSK over multipath Rayleigh fading channels (BER versus R) with $m_c = 1$ and $\beta = 200$.

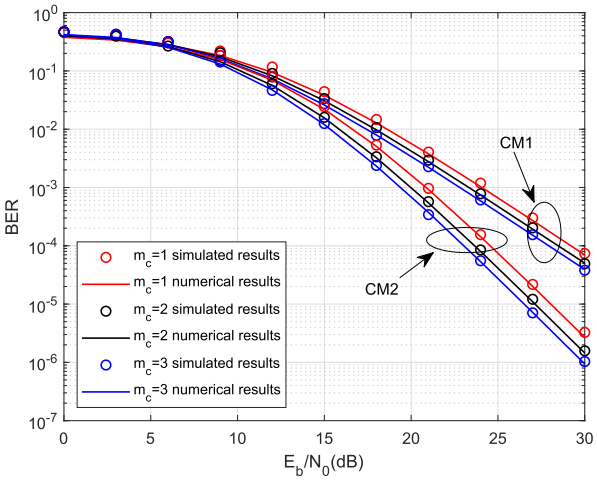

FIGURE 5. Error performance of the NR-PI-DCSK over multipath Rayleigh fading channels (BER versus m_c) with $R = 4$ and $\beta = 200$.

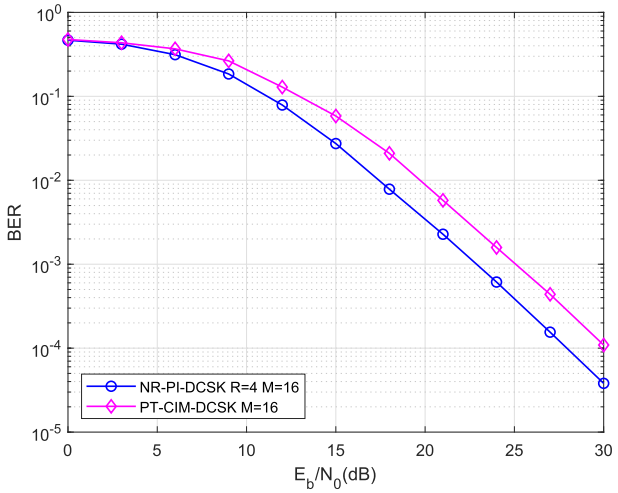

FIGURE 6. Error performance of NR-PI-DCSK and PT-CIM-DCSK over multipath rayleigh fading channels.

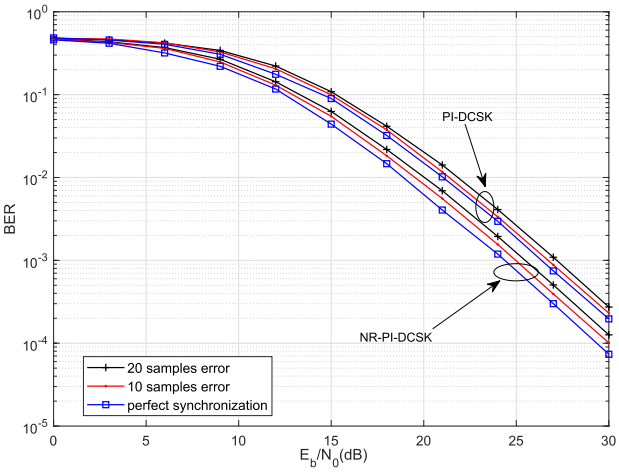

FIGURE 7. Error Performance of PI-DCSK and NR-PI-DCSK with synchronization errors.

For perfect synchronization scenario, no signal power loss under the timing mismatch, i.e., best performance can be achieved. In the case of synchronization error, the performance degradation depends on the level of symbol timing mismatch [39]. Fig. 7 further shows the error performance of the proposed NR-PI-DCSK and PI-DCSK for M=16 an $\beta = 200$ with correlation samples mismatch. We can see that as the number of mismatch samples increases, the performance becomes worse. There are about 0.5 dB and 1 dB losses as compare to the case with perfect synchronization. It is also can be seen that the proposed scheme suffers more performance loss than the PI-DCSK under the synchronization error, which leads to a smaller performance gain in this case.

To rate the BER performance of NR-PI-DCSK system over practical ultra-wideband (UWB) channel, we form the FM-NR-PI-DCSK by combining NR-PI-DCSK with the frequency-modulated (FM) structure [26]. The simulation parameters are: symbol transmission period $T_b = 500$ ns, chaotic pulse duration $T_c = 100$ ns, sampling frequency $f_s = 8$ GHz, and center frequency $f = 8$ GHz. The simulation is executed over the IEEE 802.15.4a CM7 channel based on emerging wireless industrial scenes. As demonstrated in Fig. 8, the proposed FM-NR-PI-DCSK ($R = 10$) significantly outperforms its FM-PI-DCSK counterparts by 3 dB at BER of 10^{-4} for $M = 4$. Such performance gain comes from the fact that the NR-PI-DCSK can reduce the noise level at the receiver end. Moreover, for the given parameters, Fig. 9 shows the spectrum of the chaotic signal in the proposed FM-NR-PI-DCSK. It can be seen that the flat spectrum in Fig. 9 complies with the prerequisites of Federal Communications Commission (FCC) regulations. The advantage of the NR-PI-DCSK over UWB channel is then manifested.

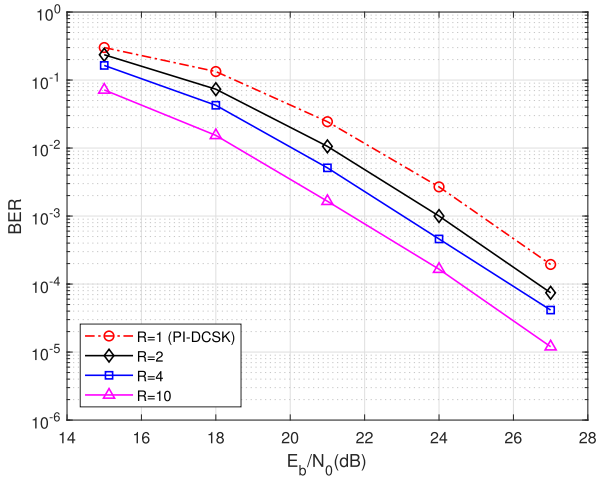

FIGURE 8. Error performance of FM-PI-DCSK and FM-NR-PI-DCSK over UWB channel.

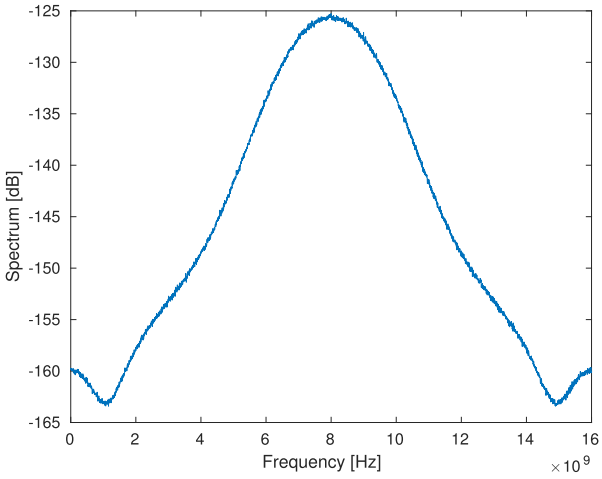

FIGURE 9. Frequency spectrum of chaotic signal in the FM-NR-PI-DCSK scheme.

V. CONCLUSION

In this paper, we propose a NR-PI-DCSK system to reduce the noise and fading interference, which leads to the increase of the received SNR. In the propose design, β/R chaotic samples are generated and then repeated R times as reference and information data are carried by the permuted replicas of the reference. We would like to note that the improperly permutation patterns result in performance degradation. This is likely to happen especially for multi-user communications, since more permutation patterns are required to assigned to the users. By doing so, the noise in the received signal can be averaged, i.e., the variance of the noise is reduced. The resultant signal is correlated with its permuted replicas to recover the data and the error performance can be improved. Moreover, we derive the analytical BER performance of the NR-PI-DCSK over multipath fading channels. Simulations show that the NR-PI-DCSK achieves significant performance gains over the conventional PI-DCSK in different wireless channel models, which has a potential to be a candidate for low-complexity short-range communications.

In addition, the proposed NR-PI-DCSK deals with the noncoherent signals to ensure the reliability performance, which increase the complexity and hardware cost. The neural network can be considered as an intelligent estimator to extract the characteristics of chaotic signals and then the transmitted data in the received signal [41]. We believe that this topic is interesting and deserves further exploration.

REFERENCES

[1] Y. Xia, C. K. Tse, and F. C. M. Lau, "Performance of differential chaos-shift-keying digital communication systems over a multipath fading channel with delay spread," *IEEE Trans. Circuits Syst. II, Exp. Briefs*, vol. 51, no. 12, pp. 680–684, Dec. 2004.

[2] R. Vali, S. Berber, and S. K. Nguang, "Accurate derivation of chaos-based acquisition performance in a fading channel," *IEEE Trans. Wireless Commun.*, vol. 11, no. 2, pp. 722–731, Feb. 2012.

[3] F. C. M. Lau, M. Ye, C. K. Tse, and S. F. Hau, "Anti-jamming performance of chaotic digital communication systems," *IEEE Trans. Circuits Syst. I, Fundam. Theory Appl.*, vol. 49, no. 10, pp. 1486–1494, Oct. 2002.

[4] M. P. Kennedy, G. Kolumban, G. Kis, and Z. Jako, "Performance evaluation of FM-DCSK modulation in multipath environments," *IEEE Trans. Circuits Syst. I, Fundam. Theory Appl.*, vol. 47, no. 12, pp. 1702–1711, Dec. 2000.

[5] J. Sun, X. Zhao, J. Fang, and Y. Wang, "Autonomous memristor chaotic systems of infinite chaotic attractors and circuitry realization," *Nonlinear Dyn.*, vol. 94, no. 4, pp. 2879–2887, Dec. 2018.

[6] Q. Xu, Y. Wang, H. Ho-Ching Iu, N. Wang, and H. Bao, "Locally active memristor-based neuromorphic circuit: Firing pattern and hardware experiment," *IEEE Trans. Circuits Syst. I, Reg. Papers*, vol. 70, no. 8, pp. 3130–3141, Aug. 2023.

[7] G. Kaddoum, F. Gagnon, P. Chargé, and D. Roviras, "A generalized BER prediction method for differential chaos shift keying system through different communication channels," *Wireless Pers. Commun.*, vol. 64, no. 2, pp. 425–437, May 2012.

[8] H. Ma, G. Cai, Y. Fang, J. Wen, P. Chen, and S. Akhtar, "A new enhanced energy-detector-based FM-DCSK UWB system for tactile internet," *IEEE Trans. Ind. Informat.*, vol. 15, no. 5, pp. 3028–3039, May 2019.

[9] F. J. Escribano, G. Kaddoum, A. Wagemakers, and P. Giard, "Design of a new differential chaos-shift-keying system for continuous mobility," *IEEE Trans. Commun.*, vol. 64, no. 5, pp. 2066–2078, May 2016.

[10] V. Mohan, A. Mathur, and G. Kaddoum, "Analyzing physical-layer security of PLC systems using DCSK: A copula-based approach," *IEEE Open J. Commun. Soc.*, vol. 4, pp. 104–117, 2023.

[11] G. Cai, Y. Fang, P. Chen, G. Han, G. Cai, and Y. Song, "Design of an MISO-SWIPT-aided code-index modulated multi-carrier M-DCSK system for e-health IoT," *IEEE J. Sel. Areas Commun.*, vol. 39, no. 2, pp. 311–324, Feb. 2021.

[12] P. Chen, L. Shi, Y. Fang, G. Cai, L. Wang, and G. Chen, "A coded DCSK modulation system over Rayleigh fading channels," *IEEE Trans. Commun.*, vol. 66, no. 9, pp. 3930–3942, Sep. 2018.

[13] Q. Chen and L. Wang, "Design and analysis of joint source channel coding schemes over non-standard coding channels," *IEEE Trans. Veh. Technol.*, vol. 69, no. 5, pp. 5369–5380, May 2020.

[14] P. Chen, L. Shi, Y. Fang, F. C. M. Lau, and J. Cheng, "Rate-diverse multiple access over Gaussian channels," *IEEE Trans. Wireless Commun.*, vol. 22, no. 8, pp. 5399–5413, Aug. 2023.

[15] Y. Fang, G. Han, P. Chen, F. C. M. Lau, G. Chen, and L. Wang, "A survey on DCSK-based communication systems and their application to UWB scenarios," *IEEE Commun. Surveys Tuts.*, vol. 18, no. 3, pp. 1804–1837, 3rd Quart., 2016.

[16] Y. Fang, "SR-DCSK cooperative communication system with code index modulation: A new design for 6G new radios," *China Commun.*, vol. 20, no. 10, pp. 1–17, 2022.

[17] G. Kaddoum, E. Soujeri, C. Arcila, and K. Eshteiwi, "I-DCSK: An improved noncoherent communication system architecture," *IEEE Trans. Circuits Syst. II, Exp. Briefs*, vol. 62, no. 9, pp. 901–905, Sep. 2015.

[18] G. Kaddoum, F.-D. Richardson, and F. Gagnon, "Design and analysis of a multi-carrier differential chaos shift keying communication system," *IEEE Trans. Commun.*, vol. 61, no. 8, pp. 3281–3291, Aug. 2013.
[19] W. K. Xu, L. Wang, and G. Kolumbán, "A novel differential chaos shift keying modulation scheme," *Int. J. Bifurcation Chaos*, vol. 21, no. 3, pp. 799–814, Mar. 2011.
[20] M. Zhang, G. Cheng, B. Yang, and C. Yang, "Generalized carrier index differential chaos shift keying based SWIPT with conversion noise and path loss-effect," *Electronics*, vol. 11, no. 15, p. 2406, Aug. 2022.
[21] M. Dawa, M. Herceg, and G. Kaddoum, "Design and analysis of multi-user faster-than-Nyquist-DCSK communication systems over multi-path fading channels," *Sensors*, vol. 22, no. 20, p. 7837, Oct. 2022.
[22] G. Kaddoum, E. Soujeri, and Y. Nijsure, "Design of a short reference non-coherent chaos-based communication systems," *IEEE Trans. Commun.*, vol. 64, no. 2, pp. 680–689, Feb. 2016.
[23] M. Mobini, G. Kaddoum, and M. Herceg, "Design of a SIMO deep learning-based chaos shift keying (DLCSK) communication system," *Sensors*, vol. 22, no. 1, p. 333, Jan. 2022.
[24] X. Cai, C. Yuen, C. Huang, W. Xu, and L. Wang, "Toward chaotic secure communications: An RIS enabled M-ary differential chaos shift keying system with block interleaving," *IEEE Trans. Commun.*, vol. 71, no. 6, pp. 3541–3558, Jun. 2023.
[25] X. Cheng, M. Zhang, M. Wen, and L. Yang, "Index modulation for 5G: Striving to do more with less," *IEEE Wireless Commun.*, vol. 25, no. 2, pp. 126–132, Apr. 2018.
[26] T. Datta, H. S. Eshwaraiah, and A. Chockalingam, "Generalized space-and-frequency index modulation," *IEEE Trans. Veh. Technol.*, vol. 65, no. 7, pp. 4911–4924, Jul. 2016.
[27] G. Cheng, L. Wang, W. Xu, and G. Chen, "Carrier index differential chaos shift keying modulation," *IEEE Trans. Circuits Syst. II, Exp. Briefs*, vol. 64, no. 8, pp. 907–911, Aug. 2017.
[28] H. Yang, S.-Y. Xu, and G.-P. Jiang, "A high data rate solution for differential chaos shift keying based on carrier index modulation," *IEEE Trans. Circuits Syst. II, Exp. Briefs*, vol. 68, no. 4, pp. 1487–1491, Apr. 2021.
[29] G. Kaddoum, M. F. A. Ahmed, and Y. Nijsure, "Code index modulation: A high data rate and energy efficient communication system," *IEEE Commun. Lett.*, vol. 19, no. 2, pp. 175–178, Feb. 2015.
[30] W. Xu and L. Wang, "CIM-DCSK: A differential chaos shift keying scheme with code-index modulation," in *Proc. Int. Symp. Commun. Inf. Technol. (ISCIT)*, 2016, pp. 100–104.
[31] H. Chen, P. Chen, Y. Fang, F. Chen, and L. Kong, "Parallel differential chaotic shift keying with code index modulation for wireless communication," *IEEE Trans. Commun.*, vol. 70, no. 8, pp. 5113–5127, Aug. 2022.
[32] M. Herceg, G. Kaddoum, D. Vranjes, and E. Soujeri, "Permutation index DCSK modulation technique for secure multiuser high-data-rate communication systems," *IEEE Trans. Veh. Technol.*, vol. 67, no. 4, pp. 997–3011, Apr. 2018.
[33] H. Chen, P. Chen, S. Wang, S. Lai, and R. Chen, "Reference-modulated PI-DCSK: A new efficient chaotic permutation index modulation scheme," *IEEE Trans. Veh. Technol.*, vol. 71, no. 9, pp. 9663–9673, Sep. 2022.
[34] Y. Fang, J. Zhuo, H. Ma, S. Mumtaz, and Y. Li, "Design and analysis of a new index-modulation-aided DCSK system with frequency-and-time resources," *IEEE Trans. Veh. Technol.*, vol. 72, no. 6, pp. 7411–7425, Jun. 2023.
[35] G. Kaddoum and E. Soujeri, "NR-DCSK: A noise reduction differential chaos shift keying system," *IEEE Trans. Circuits Syst. II, Exp. Briefs*, vol. 63, no. 7, pp. 648–652, Jul. 2016.
[36] A. Michaels, "Quantitative comparisons of digital chaotic circuits for use in communications," in *Proc. Joint INDS ISTET*, 2011, pp. 1–8.
[37] H. P. Ren, C. Bai, J. Liu, M. S. Baptista, and C. Grebogi, "Experimental validation of wireless communication with chaos," *Chaos*, vol. 26, pp. 253–261, Aug. 2016.
[38] J.-L. Yao, Y.-Z. Sun, H.-P. Ren, and C. Grebogi, "Experimental wireless communication using chaotic baseband waveform," *IEEE Trans. Veh. Technol.*, vol. 68, no. 1, pp. 578–591, Jan. 2019.
[39] Y. Kim, J. Kim, J. Kim, and J. Kang, "Comparison of DCSK receiver and enhanced DCSK receiver with synchronization error," in *Proc. IEEE Veh. Technol. Conf.*, Jul. 2006, pp. 2261–2265.
[40] J. G. Proakis, *Digital Communications Systems*. New York, NY, USA: McGraw-Hill, 2001.
[41] J. Sun, Y. Wang, P. Liu, S. Wen, and Y. Wang, "Memristor-based neural network circuit with multimode generalization and differentiation on Pavlov associative memory," *IEEE Trans. Cybern.*, vol. 53, no. 5, pp. 3351–3362, May 2023.

BINGRUI WANG received the Ph.D. degree in microelectronics and solid state electronics from the Huazhong University of Science and Technology, China, in 2015. He is currently with Nanyang Normal University. His research interests include the Internet of Things engineering and chaos-based communications.

HAOYU CHEN (Student Member, IEEE) received the B.Eng. and M.Sc. degrees from the Department of Electronic Information Engineering, Fuzhou University, Fujian, China, in 2020 and 2023, respectively. His research interests include chaos-based communications, index modulation, and their applications to wireless communications.

ZHAOPENG XIE received the Ph.D. degree in communication and information system from Fuzhou University, Fujian, China, in 2023. His primary research interests include chaos-based communications, index modulation, channel coding, physical network coding, and their applications to wireless communications.

XIAOPU MA received the Ph.D. degree in computer science and technology from the Huazhong University of Science and Technology, in 2011. He completed his postdoctoral work with the School of Automation, Huazhong University of Science and Technology, in 2015. His primary research interests include wireless communications and machine learning.

ZIQIANG ZHU received the B.S. degree in electronic information engineering from the Nanjing University of Posts and Telecommunications, Nanjing, China, in 2020, and the M.S. degree in electronic information from Fuzhou University, Fujian, China, in 2023. His primary research interests include chaotic index modulation and MIMO communications.